Neutrino absorption efficiency of an ^{40}Ar detector from the β decay of ^{40}Ti

M. Bhattacharya, A. García, and N. I. Kaloskamis*
University of Notre Dame, Notre Dame, Indiana 46556

E. G. Adelberger and H. E. Swanson
University of Washington, Seattle, Washington 98195

R. Anne, M. Lewitowicz, M. G. Saint-Laurent, and W. Trinder
GANIL, BP 5027, F-14021 Caen Cedex, France

C. Donzaud, D. Guillemaud-Mueller, S. Leenhardt, A. C. Mueller, F. Pougheon, and O. Sorlin
Institut de Physique Nucléaire, IN2P3-CNRS, F-91406 Orsay Cedex, France

(Received 4 August 1998)

We studied β-delayed proton and γ emission from ^{40}Ti decay. We found $t_{1/2}=52.7\pm1.5$ ms and observed 28 proton groups that we organized into a ^{40}Ti decay scheme with 21 branches. The reduced transition strengths of these decay branches were then used to compute the neutrino detection efficiency of the ICARUS liquid argon time-projection chamber. We found $^{40}\mathrm{Ar}(\nu,e)$ cross sections (for an electron energy threshold $W=5$ MeV) of $(14.0\pm0.3)\times10^{-43}$ cm^2, $(75.1\pm1.8)\times10^{-43}$ cm^2, and $(3.2\pm0.1)\times10^{-41}$ cm^2 for ^{8}B neutrinos, hep neutrinos, and supernova neutrinos characterized by a temperature of 4.5 MeV.
[S0556-2813(98)07812-1]

PACS number(s): 23.40.Hc, 26.65.+t, 27.40.+z

I. MOTIVATION

The proposed ICARUS II large-volume liquid-argon detector [1] has the interesting feature that it can separate neutral and charged current processes in a very symmetrical way and could definitively answer the question of solar neutrino oscillations [2,3]. In ICARUS, $e(\nu,\nu)e$ scattering interactions, which are sensitive to all neutrino flavors, will be characterized by single-track events while $^{40}\mathrm{Ar}(\nu_e,e)^{40}\mathrm{K}^*$ neutrino-nucleus interactions, which are sensitive only to electron neutrinos, will produce multiple tracks as the $J^\pi=1^+$ states fed in allowed neutrino capture emit several γ rays while cascading down to the ^{40}K $J^\pi=4^-$ ground state. Therefore the multiplicity and angular distribution of events will distinguish between neutral and charged current events.

The neutrino-electron interaction efficiency of ICARUS can be accurately calculated from electroweak theory. However, the neutrino-nucleus interaction efficiency depends on the matrix elements for neutrino-capture transitions on ^{40}Ar to excited states of ^{40}K. A recent shell-model calculation [4] predicts a capture rate of 6.7 ± 2.5 SNUs [1 SNU$=10^{-36}$ events/(sec target atom)], where 2.2 SNUs arise from the model-independent Fermi cross section and 4.5 SNUs are expected from model-dependent Gamow-Teller transitions. This strong model dependence is unusual; the efficiencies of other nuclear neutrino counters, such as the ^{37}Cl and ^{71}Ga detectors, are dominated by transitions whose strengths can be inferred from the daughter lifetime and/or from the model-independent Fermi strength. An empirical calibration of the $^{40}\mathrm{Ar}(\nu_e,e)$ transition strengths is therefore essential.

We used isospin symmetry to obtain the $^{40}\mathrm{Ar}\rightarrow{}^{40}\mathrm{K}$ transition strengths from the strengths of the mirror $^{40}\mathrm{Ti}\rightarrow{}^{40}\mathrm{Sc}$ transitions studied in ^{40}Ti β^+ decay (see Fig. 1). Our work was performed at GANIL and the first results have been published in letter form [5]. This paper presents a detailed description of our experiment and a more refined data analysis.

The β decay of ^{40}Ti also provides an opportunity to test hadronic probes of weak strength, in this case by comparing the $^{40}\mathrm{Ti}\rightarrow{}^{40}\mathrm{Sc}$ transition strengths to the forward-angle cross sections in the $^{40}\mathrm{Ar}(p,n)^{40}\mathrm{K}$ reaction. A previous comparison [6–9] of ^{37}Ca β decay to $^{37}\mathrm{Cl}(p,n)$ raised questions regarding the quantitative reliability of the charge-exchange probe; ^{40}Ti decay provides a second case where one can

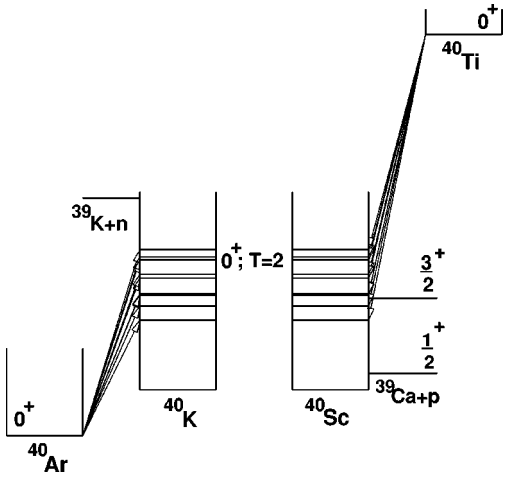

FIG. 1. Isobar diagram of the mirror processes of ^{40}Ti β^+ decay and neutrino capture on ^{40}Ar, showing only the 0^+, $T=2$ and 1^+, $T=1$ levels that can be fed in allowed transitions. Levels with unlabeled spins are known or probable 1^+ states.

*Present address: MIT-Bates Linear Accelerator Center, Middleton, MA 01949.

compare β decay and charge-exchange strengths over a wide range of excitation energies. For many cases of interest in nuclear astrophysics and neutrino physics, hadronic probes are the only empirical tool for estimating the Gamow-Teller strength; tests of these probes are essential for establishing the quantitative precision of the technique.

Little is known about ^{40}Ti as it lies far from the valley of stability. Detraz *et al.* [10] observed β delayed protons from ^{40}Ti decay, but their statistics were rather poor. They obtained a half-life of 56^{+18}_{-12} ms and observed four delayed proton branches whose branching ratios summed to $43\pm6\%$, implying that about 60% of the decays were either followed by γ rays, or by protons that were below their detection threshold. In addition their experiment suffered from two serious systematic problems. First, their implantation detector was only 118 μm thick which, for a typical implantation profile, was too thin to stop protons with $E_p>3$ MeV. Second, their proton energy threshold was quite high and degraded their detection efficiency for low-energy proton peaks. Liu *et al.* [11] recently published a study of ^{40}Ti decay (performed at GSI at about the same time as our measurement), but they observed only 11 of the 21 transitions we report in this paper.

II. EXPERIMENT

A. Apparatus

1. Production of ^{40}Ti

^{40}Ti was produced at GANIL by fragmenting a 82.6 MeV/nucleon ^{50}Cr beam on a 272.4 mg/cm^2 nickel target. The ^{50}Cr beam was produced in an ECR ion source from isotopically enriched feed material. Fragments of interest were selected by the LISE3 spectrometer with magnetic rigidities of the two dipoles set at $B\rho_1=2.012$ and $B\rho_2=1.930$ Tm, and a momentum acceptance of 1.2%. The secondary beam purity was further enhanced by a 215 μm ^{9}Be degrader foil at the intermediate focal point and by the Wien velocity filter at the exit of LISE3 [12].

2. Detection of ^{40}Ti decays

The secondary beam was sent to a counting station containing a stack of five Si surface-barrier charged-particle detectors and five 70%-efficient HPGe γ-ray detectors. The first two Si detectors (D_1 and D_2) gave energy loss (ΔE) and time-of-flight (TOF) information and provided two independent identifications of the incoming fragments. The ions were implanted in D_4 which had a thickness of 500 μm; D_4 was preceded and followed by similar 500 μm detectors, D_3 and D_5, that registered the β particles emitted by ions implanted in D_4. The ΔE signal from D_3 in conjunction with the TOF signal from D_2, provided an additional identification of the incoming fragments free from the uncertainties in the number of ions lost through reactions in D_1 and D_2.

We took roughly equal amounts of data with two different thicknesses of D_1. Data set 1 was taken with D_1 and D_2 thicknesses of 300 μm. Under these conditions the ^{40}Ti ions were implanted about 100 μm into D_4 and thus closer to D_3 than to D_5. Data set 2 was taken after replacing D_1 with a 150 μm detector so that the ^{40}Ti ions were implanted near the center of D_4.

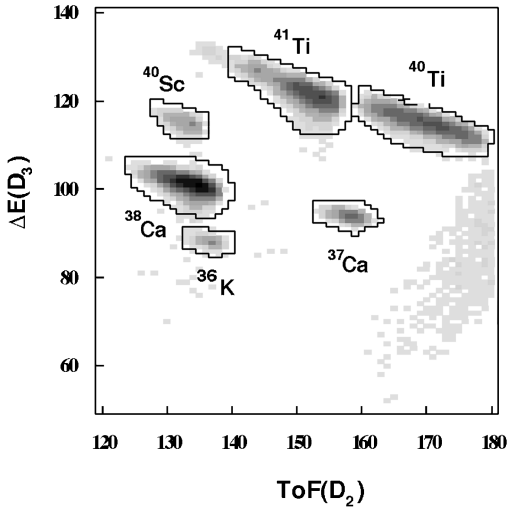

FIG. 2. Time-of-flight (D_2) vs ΔE (D_3) spectrum used to identify the implanted heavy ions. Solid lines encircle the identified ion groups.

Figure 2 shows our $\Delta E(D_3)$ vs TOF(D_2) particle identification spectrum. The groups in Fig. 2 were identified using well-established methods described elsewhere [10,12,13]. Six heavy ion species ^{41}Ti, ^{40}Sc, ^{40}Ti, ^{38}Ca, ^{37}Ca, and ^{36}K were implanted in D_4. The extended structure to the right of the ^{37}Ca group, which did not show any correlated radioactivity, was probably produced by scattered primary beam.

The number of ^{40}Ti atoms implanted in D_4 was taken as the sum of number of events in the window shown in Fig. 2, corrected for the fraction that reacted while stopping in D_4. The parametrized cross sections of Shen *et al.* [14] predict that 0.6% of the ^{40}Ti atoms reacted in D_4. We decreased the number of ^{40}Ti ions as obtained from Fig. 2 by this fraction. We checked this estimate as follows. The Shen *et al.* cross sections predict that 1.7% of the ^{40}Ti atoms observed in D_1 react before stopping in D_4. The $E(D_4)$ vs $\Delta E(D_3)$ spectrum, shown in Fig. 3, allowed us to identify the atomic numbers of the implanted ions. Requiring events to leave a Ti-ion signal in Fig. 3 reduced the number in the $\Delta E(D_1)$ vs TOF spectrum by $3\pm1\%$ in rough agreement with the calculation. The corrected number of implanted ^{40}Ti ions in data sets 1 and 2 were 30 096 and 32 495, respectively.

B. Delayed proton spectra and half-lives

We minimized contamination from other proton emitters by selecting decay events that occurred after a heavy ion of interest had been implanted in D_4 but before the arrival of the next heavy ion. In addition, we rejected events where the nucleus of interest had been implanted within a time τ after the arrival of a previous proton emitter (τ was chosen to be 5 or 10 half-lives of the previous proton emitter). The number of implanted ^{40}Ti atoms in data set 2 was reduced from 32 495 to 24 106(18 083) when we required the ^{40}Ti atoms to be implanted at least 5(10) half-lives after the previous ^{37}Ca, ^{41}Ti, or ^{40}Ti implantation.

Figure 4 shows the energy spectrum of all events in D_4 that occurred after the implantation of a ^{40}Ti ion, satisfying the condition that $\tau=5$ half-lives. Contamination from energetic, light charged particles in the beam was reduced by

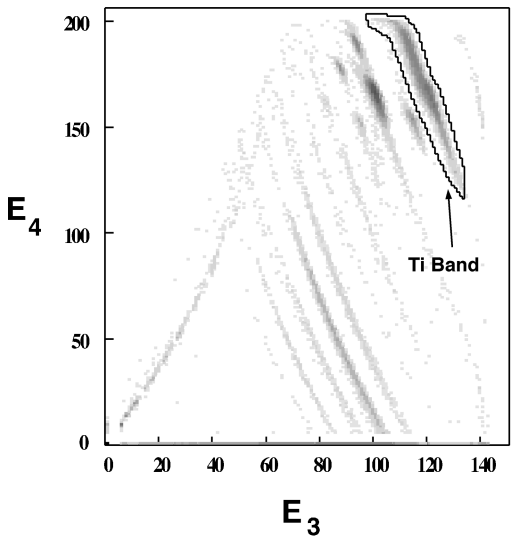

FIG. 3. E_3 vs E_4 spectrum used to verify the number of implanted heavy ions. The Ti band is identified.

rejecting events in D_4 whenever D_3 was in coincidence with D_5.

Because the waiting period for a β-delayed event was terminated whenever another proton emitter arrived, the expected rate of proton decay events in D_4 was

$$R_4(t) = \lambda \exp(-\lambda t)\exp(-\tilde{R}t), \tag{1}$$

where $\lambda = \ln 2/t_{1/2}$ and $t_{1/2}$ is the half-life of the species of interest and $\tilde{R}$ is the rate of implanted proton emitters. The first exponential in Eq. (1) is the probability that the emitter of interest did not decay until time t and the factor $\exp(-\tilde{R}t)$ is the probability that no other proton emitter arrived during the time t. From the distribution of time intervals between the successive incoming proton emitters, shown in Fig. 5, we found that $\tilde{R} = 0.769 \pm 0.003\ s^{-1}$ (the mean implantation rate of ^{40}Ti's was found to be 0.324 $\pm 0.005\ s^{-1}$ from a similar time distribution). Equation (1) is strictly valid only for constant $\tilde{R}$. However, Fig. 6, which displays the rate of incoming proton emitters as a function of time, shows fluctuations in the rate up to a factor of 2. Nevertheless, as shown in Fig. 5, the spectrum of time intervals between successive proton emitters was fitted very well by a single exponential. Monte Carlo calculations of the deduced half-lives (using the measured rates as shown in Fig. 6) showed that the correction given in Eq. (1) with the rate obtained from Fig. 5 yielded the correct half-lives.

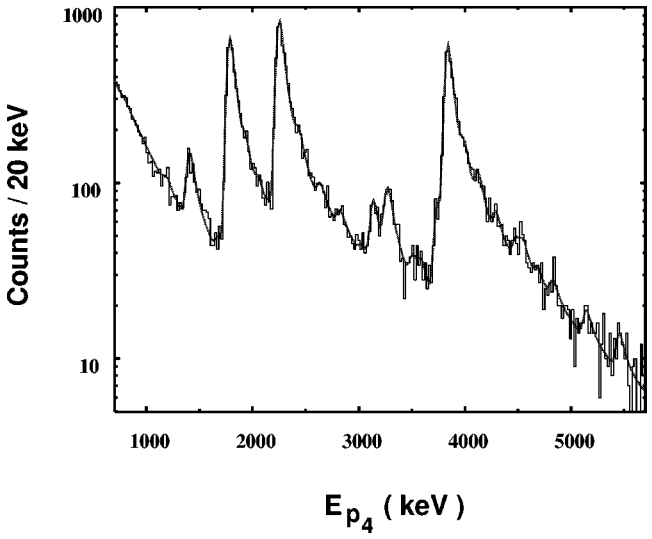

FIG. 4. Energy spectrum of decay events in D_4 following implantations of ^{40}Ti ions. Our fit to this spectrum from data set 2 is shown.

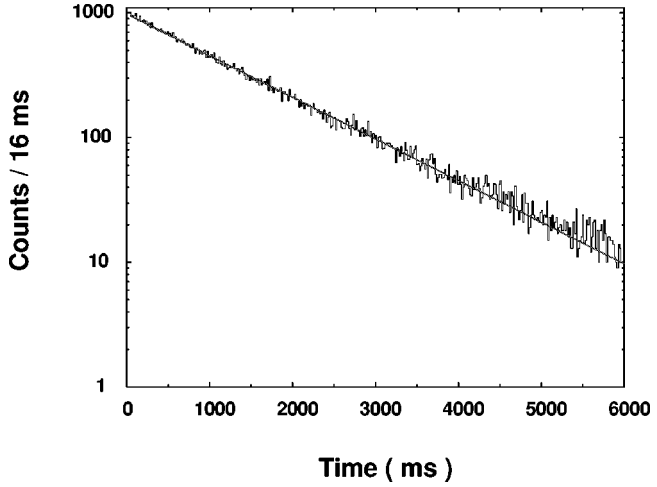

FIG. 5. Distribution of time intervals between successive heavy-ion implantations. This was used to correct half-lives and branching ratios for early gate closing. The fit to the data is shown.

Because we stopped waiting for decay products after another proton emitter was implanted, our decay branching ratios are corrected by the same effective live fraction as the half-lives:

$$F(\lambda) = \frac{\int_0^\infty \exp(-\lambda t)\exp(-\tilde{R}t)dt}{\int_0^\infty \exp(-\lambda t)dt} = \frac{\lambda}{\lambda + \tilde{R}}. \tag{2}$$

Another source of dead-time, which affected the branching ratios but not the extracted half-life, was the very large

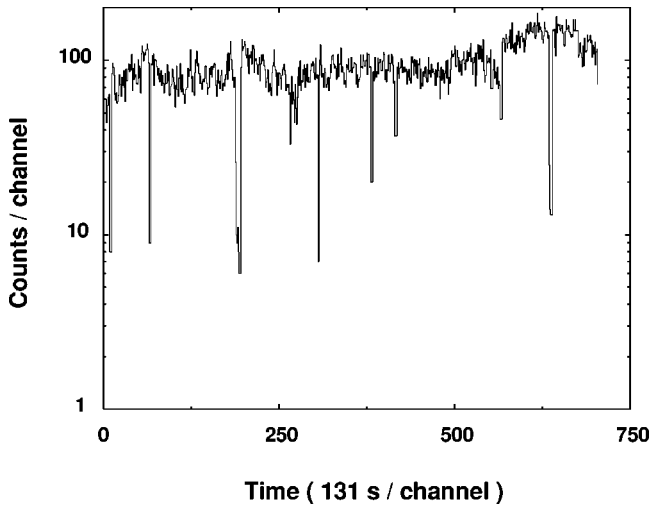

FIG. 6. Distribution of the absolute time of incoming proton emitters. The spikes are artifacts created at the beginning and end of individual runs.

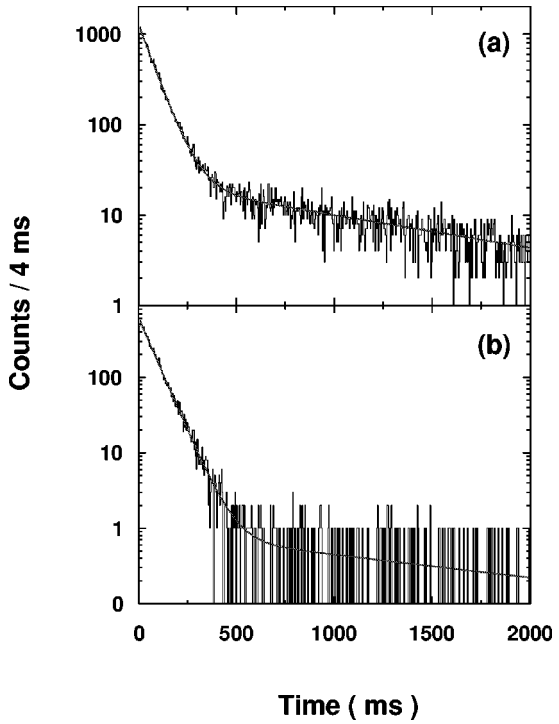

FIG. 7. (a) Distribution of time intervals between implantation of a ^{40}Ti ion and a subsequent $E_p^{\rm lab}>800$ keV event in D_4. The curve is a fit to the data. (b) The same distribution as in (a) except that the decay events in this case were required to be in coincidence with a β particle in D_3 or D_5. The curve is a fit of to the data. The deficiency of counts for intervals <8 ms is due to electronic and computer dead time.

pulse produced in D_4 when a heavy ion was implanted. This made the detector insensitive for the next ≈ 3 ms. The effect is noticeable at early times in Figs. 7(a) and 7(b). We eliminated uncertainties from this effect by incrementing the proton spectrum only for events that occurred at least 4 ms after the heavy-ion implantation and correcting for events lost during this imposed dead time. This correction increased the ^{40}Ti peak areas by $5.4\pm0.5\%$.

Figure 7(a) shows the distribution of time intervals between implantation of a ^{40}Ti arriving at least five half-lives after the preceding proton emitter, and a subsequent decay event in D_4 with $E_4>800$ keV. The long-lived component in this spectrum is due to β's from ^{38}Ca atoms implanted before the ^{40}Ti (no requirement was placed on the time difference between the implantations of ^{40}Ti and the previous ^{38}Ca) and energetic light charged particles that escaped the anticoincidence condition with D_3 and D_5. The data are well fitted by the sum of two exponentials. Figure 7(b) shows the corresponding distribution of time intervals for decay events leaving an energy $E_4>1565$ keV in D_4, which reduced the contamination from ^{38}Ca β's. The decay events in this spectrum were required to be in coincidence with >800 keV signals in D_3 or D_5 to reduce noise. As the long-lived component in Fig. 7(b) has poor statistics, we fitted this spectrum with two exponentials using a maximum likelihood routine with Poisson statistics. Because the distributions were terminated if another proton emitter was implanted before the proton decay occurred, the half-lives obtained from fitting these spectra were corrected according to Eq. (1). From these data we extract a ^{40}Ti half-life of 53.6 ± 0.6 ms. We average this half-life with the value 51.7 ± 0.6 ms obtained in Ref. [5] from a completely independent analysis of the same data. We adopt a half-life of 52.7 ± 1.5 ms which encompasses 68% of the probability from the sum of two Gaussian distributions representing the two independent analyses. This agrees with the values in Ref. [10], 56^{+18}_{-12}, and Ref. [11], 55.0 ± 2.0, and with the shell-model prediction [4] of 55 ± 5 ms. These same procedures applied to our ^{41}Ti and ^{37}Ca data gave half-lives of 81.3 ± 2.0 ms and 188.7 ± 20.5 ms respectively which can be compared to their presently accepted values of 80.0 ± 2.0 ms [15] and 181.1 ± 1.0 ms [8], respectively (Table I).

TABLE I. β-decay half-lives extracted from this experiment and other work.

	$t_{1/2}$ (ms)	
Parent	This work[a]	Previous work
^{40}Ti	52.7 ± 1.5	$56.0^{+18.0}_{-12.0}$ [b]
		55.0 ± 2.0[c]
^{41}Ti	81.3 ± 2.0	80.0 ± 2.0[d]
^{37}Ca	188.7 ± 20.5	181.1 ± 1.0[e]

[a]Extracted from ions implanted at least five half-lives after the previous proton emitter. The result is corrected for heavy-ion induced dead-time as discussed in the text.
[b]From Ref. [10].
[c]From Ref. [11].
[d]From Ref. [15].
[e]From Ref. [8].

1. Line shape analysis

The tails on the proton groups in Fig. 4 arose from summing of protons with the preceding positrons. The fitted line shapes in Fig. 4 were generated using Monte-Carlo simulations that approximated the implantation profile as a Gaussian with 55 ± 5 μm full width at half maximum (FWHM) (dominated by the finite energy acceptance of the spectrometer) with a mean depth of 258 μm (calculated using the code LISE [13]). We checked that the ^{40}Ti's were implanted in the center of D_4 by comparing the centroids of proton groups coincident with β's in D_3 and D_5. The centroid difference of 12.0 ± 6.3 keV, implied an implantation centroid at 266 ± 17 μm, in agreement with the LISE calculation. The simulations assumed that positrons were emitted isotropically and deposited an energy that depended on their straight-line path lengths from the point of emission to the surface of the detector. The energy deposited was found by parametrizing Bichsel's [16] predicted electron energy loss distribution in silicon for incident energies of 1, 3, 5, 7, and 9 MeV and silicon thicknesses of 50, 62.5, 100, 125, 200, 250, 400, and 500 μm. The code then chose a random direction for the emitted proton and calculated the energy deposited by the proton using Bichsel's dE/dx values for protons in silicon. The simulation predicted that the efficiency for observing a sharp proton line was essentially unity for transitions with $E_p^{\rm lab}<5$ MeV but that the yields for the last two transitions in Table II should be increased by 1 and 3 counts, respectively.

TABLE II. β-delayed proton groups from ^{40}Ti decay. These results were obtained from 24 106 ^{40}Ti's implanted at least five half-lives after the preceding proton emitter. Peaks in parentheses improved the total χ^2 by more than two and less than four units.

E_p^{lab}(MeV)	E_x(^{40}Sc)(MeV)	Peak area[a]
0.747±0.036[b]	3.775±0.046	117±41
1.111±0.020[b]	4.149±0.028	128±32
1.325±0.007[b]	4.367±0.010	864±145
1.608±0.017[b]	4.658±0.023	92±43
1.701±0.006	2.281±0.008	5728±142
1.849±0.014[b]	4.904±0.019	341±77
1.957±0.021[b]	5.015±0.027	206±63
2.027±0.028[b]	5.086±0.036	107±27
2.160±0.006	2.752±0.008	7183±158
2.341±0.010	2.937±0.013	468±98
2.542±0.016	3.143±0.020	219±50
2.728±0.016	3.334±0.019	140±42
(2.957±0.047)	(3.569±0.056)	(26±26 [c])
3.039±0.008	3.652±0.010	417±48
3.170±0.008	3.786±0.010	504±55
(3.242±0.041)	(3.861±0.049)	(26±26 [c])
3.443±0.021	4.067±0.024	104±34
3.487±0.025	4.111±0.030	79±34
3.639±0.008	4.267±0.010	494±53
3.734±0.007	4.364±0.008	5233±129
3.887±0.011	4.522±0.012	442±68
4.017±0.010	4.655±0.012	383±55
4.184±0.018	4.825±0.021	173±40
4.371±0.023	5.017±0.027	128±55
4.433±0.031	5.080±0.035	101±57
(4.572±0.028)	(5.223±0.032)	(27±27 [c])
5.034±0.020	5.696±0.023	57±21
5.336±0.019	6.006±0.021	50±17

[a]Peak areas are corrected for early gate closing and electronic dead times.

[b]Decay leaving ^{39}Ca in its first excited state.

[c]The uncertainties in the intensities for these transitions have been inflated to make them consistent with zero.

The resulting line shape, shown in Fig. 8, represented, for a given level in ^{40}Sc, the energy left in D_4 by the proton and the positron. This line shape was then folded with a Gaussian that accounted for detector noise. We fitted the spectra with these line shapes plus a linear background and a rise at zero energy (the rise accounted for β decays not followed by protons, e.g., ^{38}Ca, and for other particles that may have been in the secondary beam) using the Levenberg-Marquardt method [17,18].

Figure 4 shows our fit to the ^{40}Ti data for set 2 and Table II gives the areas of the 28 observed ^{40}Ti proton groups. The proton spectrum in coincidence with a β particle in D_3 from data set 1, shown in Fig. 9, yielded a higher resolution spectrum (with lower statistics) because the ions were implanted closer to D_3. We used this spectrum to obtain the relative intensities and the peak positions for transitions with E_p^{lab} <5 MeV which were then used as starting values when fitting data set 2. Additional peaks were added at $E_p^{lab}>5$ MeV to fit observed structures at these energies. We obtained the peak areas and centroids by minimizing χ^2 $[(\chi^2/\nu)_{min}$ $=1.18$ and $\nu=234]$ for the entire spectrum. The total χ^2 for the entire spectrum was required to improve by at least four units for a structure to be assigned as a definite peak. Peaks that improved the χ^2 by 2 to 4 units are shown in parentheses in Tables II and III.

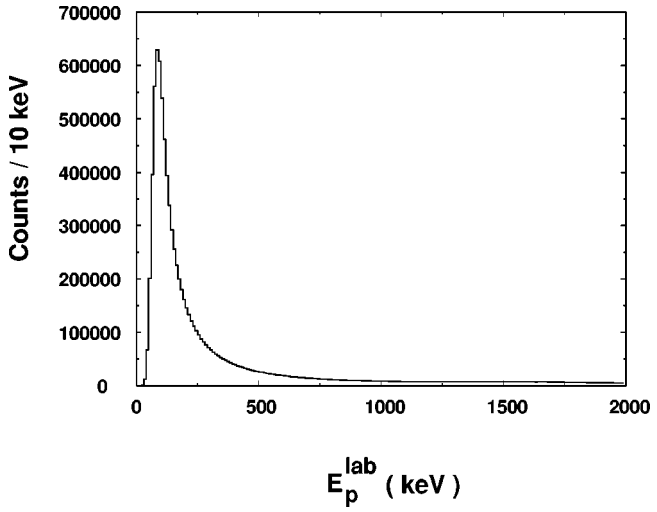

FIG. 8. Monte Carlo prediction for the delayed-proton line shape of a transition to a ^{40}Sc state.

We fitted our ^{41}Ti data with the same line shapes used for ^{40}Ti. Except for a proton group at $E_p^{lab}=1530\pm8$ keV, our intensities, shown in Table IV, agree well with recent data of Honkanen *et al.* [19]. Neither we nor Honkanen *et al.* resolved the 1530 keV peak from a lower intensity peak. Because Ref. [19] only covered proton peaks up to E_p^{lab} $=4736$ keV, we compare our groups with $E_p^{lab}>4736$ keV to the earlier data of Sextro *et al.* We observe significant discrepancies for the intensities of groups at $E_p^{lab}=4827\pm10$ and 4954 ± 11 keV. These discrepancies probably arose because Sextro *et al.*'s data contained β-delayed protons from ^{25}Si, ^{37}Ca, and ^{40}Sc as well as from ^{41}Ti.

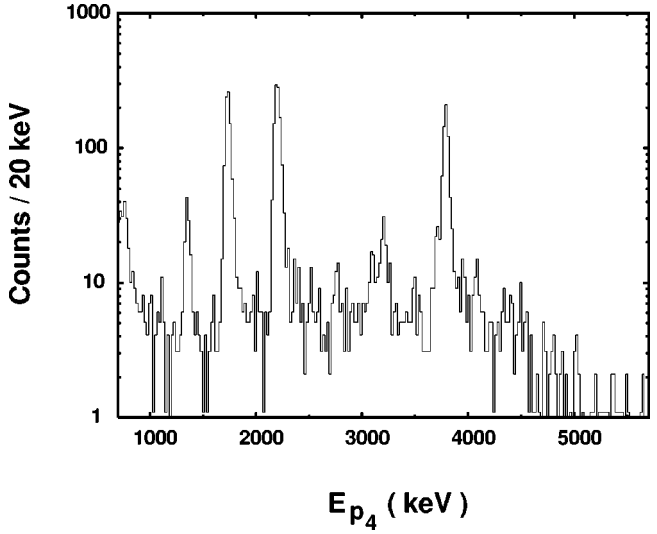

FIG. 9. Energy spectrum of ^{40}Ti decays in D_4 gated by β pulses in D_3. Results are from data set 1.

TABLE III. ^{40}Ti β^+ decay branches.

This work		Liu *et al.*[a] [11]	
E_x(keV)	B(%)	E_x(keV)	B(%)
		1750±20[c]	1.1±0.6
2281±8	23.78±0.61	2300±10	26.0±3.0
		2570±20[c]	0.6±0.3
2752±8	29.82±0.69	2770±10	32.0±3.0
2937±13	1.95±0.41		
3143±20	0.91±0.21	3100±20	1.3±0.7
3334±19	0.58±0.17	3350±20	1.0±0.5
(3569±56)	(0.11±0.11)		
3652±10	1.73±0.20		
3786±10[b]	2.58±0.29	3760±10	4.7±0.5
(3861±49)	(0.11±0.11)		
4067±24	0.43±0.14		
4111±30[b]	0.86±0.19		
4267±10	2.05±0.22		
4364±8[b]	25.32±0.82	4370±10	31.0±3.0
4522±12	1.85±0.28		
4655±12[b]	1.97±0.29		
4825±21[b]	2.14±0.36	4780±20	0.9±0.5
5017±27[b]	1.39±0.35		
5080±35[b]	0.86±0.26	5070±20	1.1±0.6
(5223±32)	(0.11±0.11)	(5360±20)	(0.4±0.2))
5696±23	0.24±0.09	>5500	0.7±0.2
6006±21	0.21±0.07		
Total	99.00±1.59		100.8±5.4

[a]Listed simply in order of increasing excitation energy.
[b]Daughter state decaying to both the ground and first excited states of ^{39}Ca. The remaining transitions fed only the ^{39}Ca ground state.
[c]Ref. [11] assigned these groups to p_0 decays. We believe this is incorrect; we assign our corresponding groups to p_1 decays.

2. Proton energy calibration

We calibrated the D_4 energy scale by fitting our ^{41}Ti peak centroids (excluding the 1530 keV peak) with the energies from Ref. [19], using a linear regression routine with errors in both variables to minimize χ^2 [$(\chi^2/\nu)_{\min}\approx 0.59$]. The resulting fit is shown in Fig. 10. Because our calibration was made with a source (^{41}Ti) whose mass and implantation profile were similar to those of the ^{40}Ti ions of interest, we automatically corrected for the energy deposited by the recoiling daughter.

C. Delayed γ spectra

We determined the Ge detector efficiencies using calibrated γ-ray sources, and checked them on-line by counting the 1568 keV γ rays from implanted ^{38}Ca ions. The summed photopeak efficiency of the five Ge detectors was $\eta = 1.12 \pm 0.11\%$ at $E_\gamma \approx 2470$ keV. Figure 11 shows the summed γ-ray spectrum gated by a $>$ 800 keV signal in D_4 following the implantation of a ^{40}Ti ion. The peak at $E_\gamma = 2471$ keV arises from proton decays that left ^{39}Ca in its first excited state (i.e., p_1 decays). Figure 12 shows β-delayed protons from ^{40}Ti decay in coincidence with the 2471 keV γ ray. The figure shows coincidences for proton peaks with $E_p^{\rm lab}$

TABLE IV. Delayed proton groups from ^{41}Ti decay.

This work		Refs. [19,20][a]	
$E_p^{\rm lab}$(keV)	B(%)	$E_p^{\rm lab}$(keV)	B(%)
698±45	0.3±0.1	754±12	0.3±0.1
985±7	5.3±0.3	986±5	5.1±0.5
1538±7	2.3±0.2	1542±2	7.5±0.7
1594±25	0.4±0.1	1586±11	1.0±0.2
1947±26	0.4±0.1	1981±12	0.7±0.2
2278±7	4.1±0.2	2270±4	4.7±0.5
2412±8	2.5±0.2	2414±3	2.2±0.3
2658±12	0.8±0.2	2650±12	1.8±0.3
2800±12	0.6±0.2	2796±14	0.6±0.2
3087±7	16.5±0.8	3083±5	17.2±1.0
3158±18	1.5±0.6	3139±12	0.7±0.2
3352±15	0.8±0.2	3330±13	0.6±0.2
3488±16	0.7±0.2	3480±12	0.6±0.2
3604±11	1.5±0.2	3598±6	1.9±0.3
3691±10	3.3±0.6	3691±5	4.7±0.5
3751±8	6.7±0.6	3749±5	7.6±0.6
3803±18	1.0±0.3	3837±9	0.9±0.2
3870±15	0.9±0.2	3888±11	0.8±0.2
4185±8	3.8±0.2	4189±6	3.4±0.4
4323±32	0.4±0.2	4298±13	0.3±0.2
4397±11	1.4±0.2	4381±8	1.6±0.2
4586±15	0.7±0.2	4564±20	0.6±0.1
4634±8	3.9±0.8	4639±5	5.0±0.5
4666±36	1.2±0.3	4684±11	1.1±0.2
4736±8	26.6±1.1	4736±4	26.1±1.0
4829±11	3.3±0.7	4832±25	0.8±0.1
4877±36	1.0±0.3	4876±20	0.9±0.1
4949±14	1.9±0.5	4925±20	0.8±0.1
5165±17	1.5±0.5	5177±30	0.8±0.1
Total	95.3±2.3		100.3±2.2

[a]Peaks with $E_p^{\rm lab} \leqslant 4736$ keV from Ref. [19], peaks with $E_p^{\rm lab} > 4736$ keV from Ref. [20].

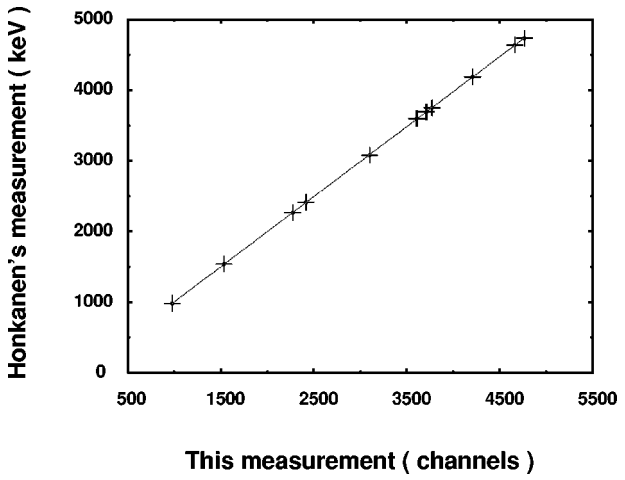

FIG. 10. Proton energy calibration of D_4 obtained from ^{41}Ti decay. Peak energies are taken from Honkanen *et al.* The fit to the data is shown.

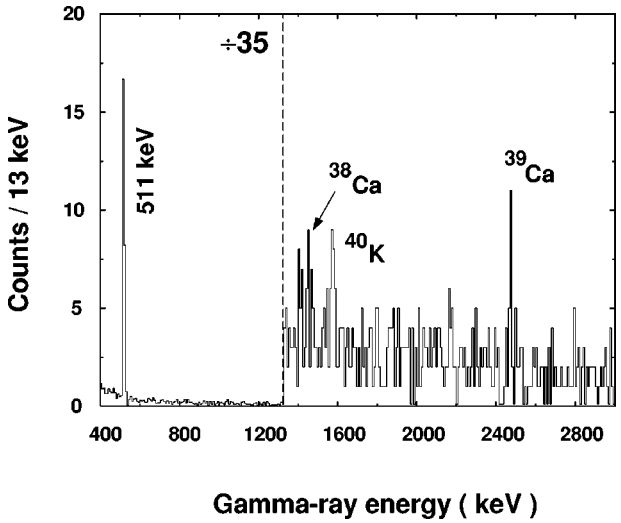

FIG. 11. γ-ray spectrum in coincidence with a beta event following the implantation of a ^{40}Ti ion, obtained by combining the results from five separate Ge detectors.

$\approx$1320, 1620, and 2030 keV and shows no evidence for accidental coincidences (which would have the same structure as that of the singles spectrum but with diminished statistics).

Of the three proton peaks showing coincidences, the peak at $E_p^{\rm lab} \approx 1320$ keV shows 9 ± 3 counts, in agreement with the number of counts one would expect from the intensity of the proton group at $E_p^{\rm lab}=1325\pm7$ keV in the singles spectrum and our detection efficiency for the 2471 keV γ ray. The corresponding excitation energy, 4367 ± 10 keV, indicates a p_1 decay of the ^{40}Sc IAS. The poor statistics in Fig. 12 prevented us from determining with certainty whether any other proton groups were in coincidence with 2471-keV γ's. We assigned the proton groups at $E_p^{\rm lab}=747\pm36$, 1111 ± 20, 1608 ± 17, 1849 ± 14, 1957 ± 21, and 2027 ± 28 keV to p_1 decays for the following reason. If these groups came from p_0 decays, they would imply the existence of 1^+ states in ^{40}Sc at $E_x=1304\pm46$, 1678 ± 28, 2187 ± 23, 2433 ± 19, 2544 ± 27, and 2615 ± 36 keV, respectively. No analogous 1^+ levels are seen in the well-studied ^{40}K mirror nucleus. On the other hand, if these groups arose from p_1 decays, the corresponding excitation energies $E_x=3775\pm46$, 4149 ± 28, 4658 ± 23, 4904 ± 19, 5015 ± 27, and 5086 ± 36 keV, agree well with p_0 decays observed in our work. We assign the remaining 21 proton groups to p_0 decays. We checked that our p_1-decay assignments agreed with our proton-γ coincidence data by comparing a model using the p_1-decay intensities shown in Table II and the proton line shape described before to the proton spectrum gated by 2471-keV γ's, which yielded $\chi^2/\nu=0.21$.

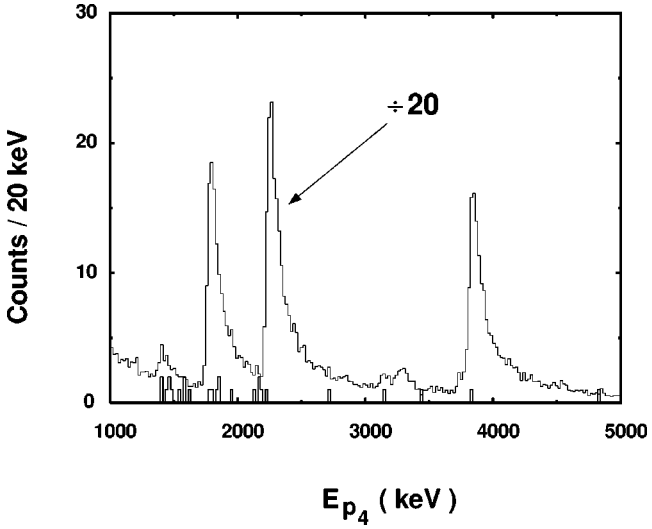

FIG. 12. ^{40}Ti proton spectrum in coincidence with 2471 keV γ rays compared to the proton singles spectrum.

TABLE V. Masses of the lowest $T=2$ quintet in $A=40$.

Nucleus	T_z	Mass excess[a] (keV)
^{40}Ar	2	-35039.889 ± 0.004
^{40}K	1	-29151.00 ± 0.27
^{40}Ca	0	-22858.11 ± 2.02
^{40}Sc	-1	-16161.9 ± 8.9[b]
^{40}Ti	-2	-8850 ± 160

[a]Using accepted values for ground-state masses [22] and E_x's [15] unless otherwise noted.
[b]Delayed proton energy from this work, plus Ref. [22].

The lowest $T=2$ level in ^{40}K decays by γ emission to 1^+ states at 2290 and 2730 keV with branching ratios of $76\pm3\%$ and $24\pm3\%$, respectively [15,21]. Isospin symmetry predicts that the ^{40}Sc level should have identical reduced $M1$ transition strengths and hence similar relative γ-ray branching ratios. Because of our relatively low γ-ray efficiency, we can set only an upper limit of 1.1% on the β-delayed γ decays of the $T=2$ level, corresponding to $\Gamma_\gamma/(\Gamma_{p0}+\Gamma_{p1})\leqslant0.043$. Assuming identical isospin-reduced matrix elements in ^{40}Sc and ^{40}Ca, we obtain $\Gamma_\gamma(^{40}{\rm Sc}, T=2)=3/4\,\Gamma_\gamma(^{40}{\rm Ca}, T=2)$. The observed width in ^{40}Ca, $\Gamma_\gamma=0.74\pm0.06$ eV [15], implies $\Gamma_\gamma(^{40}{\rm Sc}, T=2)=0.56\pm0.05$ eV and $\Gamma_p(^{40}{\rm Sc}, T=2)\geqslant13.0$ eV.

We saw no clear evidence for β transitions followed *only* by γ rays. We fitted the time spectrum gated by the beta energy region in the D_4 spectrum with two exponentials. When the half-life of one exponential was fixed to that of ^{40}Ti we obtained a 1.2% upper limit on the total intensity of ^{40}Ti β decays followed only by γ decays.

D. ^{40}Ti mass and the β-decay energy release

Because the β-decay phase-space factor is a strong function of the end-point energy, which in turn depends on the ^{40}Ti mass, the ±160 keV uncertainty in the tabulated ^{40}Ti mass [23] produces a large uncertainty in the phase space factor. We circumvented this problem by using the isobaric multiplet mass equation (IMME) [22,24] to predict the ^{40}Ti mass from the precisely known masses of the other four members of the $A=40$, $T=2$ quintet. Table V shows the masses and Table VI shows the results of fits including quadratic, cubic, and quartic polynomials in T_3. As expected, there is no evidence for cubic or quartic terms. The usual quadratic expression yields a ^{40}Ti mass excess of -9060 ± 10 keV, which can be compared to the measured value of

TABLE VI. IMME coefficients for the lowest $T=2$ multiplet in $A=40$.

a (keV)	b (keV)	c (keV)	d (keV)	e (keV)	χ^2/ν	P(χ^2/ν)
-22858.0 ± 1.7	-6495.0 ± 2.5	202.0 ± 0.9			0.87	0.42
-22858.3 ± 2.0	-6495.4 ± 3.1	203.1 ± 4.8	-0.6 ± 1.7		1.68	0.19
-22858.0 ± 2.0	-6495.0 ± 4.4	202.0 ± 5.7		0.0 ± 0.9	1.74	0.18
-22858.1 ± 2.0	-6477.0 ± 15.0	193.0 ± 9.0	-18.0 ± 13.0	9.0 ± 7.0		

-8850 ± 160 keV [22]. The IMME prediction implies $Q_{EC}=11466\pm11$ keV, which we used when calculating the phase space factors.

E. Branching ratios and transition strengths

Our ^{40}Ti β^+ branching ratios, which sum to $99.00\pm1.59\%$, are given in Table III, along with the results of previous measurements [11]. We assumed that all lines arose from single-proton decays of ^{40}Sc. In principle, ^{40}Sc levels above 6.03 MeV can emit two protons. However, Coulomb penetrabilities significantly hinder transitions with proton energies less than 1 MeV, so ^{40}Sc levels below 7 MeV should not decay appreciably by this mode.

Table VII compares the excitation energies of our ^{40}Sc daughter levels to the energies of known or probable [15] $1^+;1$ and $0^+;T=2$ levels in ^{40}K, and also shows the reduced transition strengths B_i for populating these levels in ^{40}Ti decay. The reduced transition strengths were computed as

$$B_i(\mathrm{GT})+B_i(\mathrm{F})=K\frac{B_i}{f(\mathrm{E}_i)\,t_{1/2}}, \tag{3}$$

where $K=6127\pm9$ s [25], E_i is the β-end-point energy and $f(E_i)$ the phase space factor [26]. Figure 13 shows the integrated Gamow-Teller strength as a function of ^{40}Sc excitation energy. The B value for the analog transition, 3.84 ± 0.17, which is marginally less than the expected value of 4, indicates that $(4.0\pm4.3)\%$ of the Fermi strength is mixed into other 0^+ levels.

TABLE VII. β decay of ^{40}Ti and the neutrino-capture cross section of ^{40}Ar. (Cross sections for ^{8}B and supernova ν's are computed with a 5 MeV threshold on the total energy of the outgoing electron.) The isobaric correspondences suggested in this table are based solely on excitation energies and J^π assignments.

E_x(keV)(^{40}Sc)	B(F)+B(GT)	E_x(keV)(^{40}K)	J^π(^{40}K)[a]	$\sigma_B(10^{-43}\mathrm{cm}^2)$[b]	$\sigma_{SN}(10^{-43}\mathrm{cm}^2)$[c]
2281 ± 8	0.90 ± 0.04	2289.88 ± 0.03	1^+	3.19 ± 0.14	38.04 ± 1.69
2752 ± 8	1.50 ± 0.06	2730.38 ± 0.04	1^+[d]	4.14 ± 0.14	59.86 ± 2.00
2937 ± 13	0.11 ± 0.02	2950.70 ± 0.50		0.27 ± 0.05	4.28 ± 0.78
3143 ± 20	0.06 ± 0.01	3109.75 ± 0.04	$(1,2)^+$	0.13 ± 0.02	2.29 ± 0.38
3334 ± 19	0.04 ± 0.01	3146.44 ± 0.09	1	0.09 ± 0.04	1.52 ± 0.76
3569 ± 56	0.01 ± 0.01	3293 ± 10		0.02 ± 0.02	0.37 ± 0.37
3652 ± 10	0.16 ± 0.02	3738.50 ± 0.05	1^+	0.24 ± 0.02	5.62 ± 0.35
3786 ± 10	0.26 ± 0.03	3797.58 ± 0.06	1^+	0.39 ± 0.03	9.06 ± 0.70
3861 ± 49	0.01 ± 0.01	3840.25 ± 0.05	$(1,2)^+$	0.02 ± 0.02	0.35 ± 0.35
4067 ± 24	0.05 ± 0.02	3898 ± 8		0.07 ± 0.03	1.72 ± 0.69
4111 ± 30	0.11 ± 0.03	3996 ± 10	U	0.14 ± 0.03	3.74 ± 0.68
4267 ± 10	0.29 ± 0.03	4352 ± 5	U	0.28 ± 0.03	9.38 ± 0.97
4364 ± 8	3.84 ± 0.17	4384.00 ± 0.30	$0^+;2$	3.75 ± 0.17	124.07 ± 5.49
4522 ± 16	0.31 ± 0.05	4697 ± 10	U	0.24 ± 0.04	9.57 ± 1.54
4655 ± 12	0.38 ± 0.06	4761 ± 5	$(1,2)^+$	0.27 ± 0.04	11.64 ± 1.53
4825 ± 21	0.47 ± 0.08	4788.65 ± 0.17	1^+	0.33 ± 0.06	14.34 ± 2.44
5017 ± 27	0.36 ± 0.09	4848 ± 10		0.24 ± 0.06	10.91 ± 2.73
5080 ± 35	0.23 ± 0.07	5027 ± 5		0.13 ± 0.05	6.80 ± 2.36
5223 ± 32	0.03 ± 0.03			0.02 ± 0.02	0.87 ± 0.87
5696 ± 23	0.11 ± 0.04			0.03 ± 0.01	2.97 ± 1.08
6006 ± 21	0.13 ± 0.05			0.03 ± 0.01	3.37 ± 1.30
Total	9.36 ± 0.26			14.02 ± 0.30	320.77 ± 8.27

[a]U denotes unnatural parity.

[b]For the standard ^{8}B ν_e spectrum of Ref. [28].

[c]For supernova ν_e's with $T=4.5$ MeV.

[d]The positive parity assignment follows from the strong population of its ^{40}Sc analog in ^{40}Ti decay.

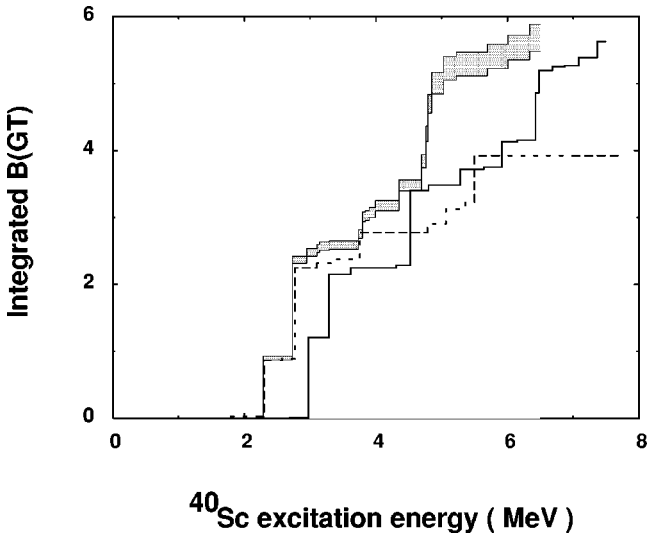

FIG. 13. Integrated B(GT) strength for ^{40}Ti decay as a function of E_x. The shaded region shows the 1σ errors from this experiment. The solid line shows the shell-model prediction of Ref. [4] and the dashed line shows the data from Ref. [11].

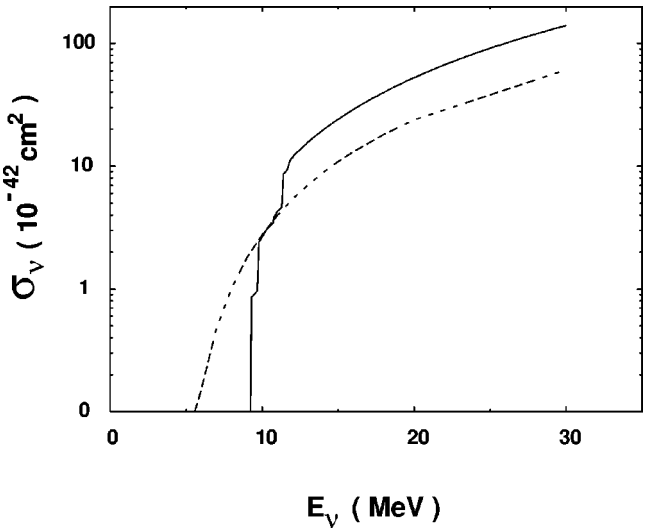

FIG. 14. Neutrino absorption cross section of ^{40}Ar as a function of incident neutrino energy. The solid curve is for a $W=5$ MeV threshold on the outgoing electron. The discontinuities in the cross section occur because we assumed a sharp threshold. The dashed curve shows the corresponding efficiency [29] for the ^{37}Cl detector.

III. NEUTRINO ABSORPTION CROSS SECTION ON ^{40}Ar

In the allowed approximation, the neutrino absorption cross section on ^{40}Ar is given by

$$\sigma(E_\nu)=\frac{G_F^2\cos^2\theta_{ud}}{\pi\hbar^4c^3}\sum_i p_iW_iF(Z,W_i)[B_i(GT)+B_i(F)]. \tag{4}$$

The sum runs over all ^{40}K daughter levels, $G_F\cos\theta_{ud}$ is the β-decay vector coupling constant [26], p_i and W_i refer to the momentum and total energy of the outgoing electron, and $F(Z,W)$ accounts for the Coulomb distortion of the outgoing electron wave function. We computed $\sigma(E_\nu)$ for the neutrino-capture reactions using the B_i values of the isospin-analog β decays of ^{40}Ti given in Table VII. We calculated $F(Z,W)$ using our codes for F_0 and screening corrections and by interpolating Behrens and Jänecke's [27] L_0 value (their Table II) for finite-size corrections. The excitation energies of the ^{40}K final states are shown in Table VII; when the ^{40}K analog of the ^{40}Sc β-decay daughter could not be found, we used the ^{40}Sc energy instead. Figure 14 shows the ^{40}Ar ν-absorption cross section as a function of the neutrino energy for an electron total-energy threshold of $W=5$ MeV [1]. Figure 14 also shows the total absorption cross section for the radiochemical ^{37}Cl detector. The ^{40}Ar(ν,e) reaction has roughly twice the cross section of the ^{37}Cl(ν,e) reaction for $E_\nu\geq 10$ MeV.

We have integrated ^{40}Ar$(\nu_e,e)^{40}$K* cross section from Fig. 14 over the standard (no neutrino oscillations) ^{8}B [28] and hep [29] neutrino spectra. The total capture cross section for ^{8}B neutrinos, $(14.0\pm0.3)\times10^{-43}$ cm^2, is about 22% higher than Ormand *et al.*'s calculation, primarily because the predicted daughter-state excitation energies are 0.2 to 1 MeV higher than the measured values. The total capture cross-section for hep neutrinos is $(75.1\pm1.8)\times10^{-43}$ cm^2. ICARUS II will also be useful as a detector of supernova neutrinos. We obtain a total absorption cross section of $(3.2\pm0.1)\times10^{-41}$ cm^2 for ν_e's from a Fermi-Dirac energy distribution with $T\approx4.5$ MeV. This implies that a 5000 ton detector could see ≈275 absorption events from a supernova with the characteristics of SN1987A. The sensitivity of the ICARUS efficiency to the energy threshold on the outgoing electron is shown in Table VIII.

Three sources of systematic error in these cross-section calculations deserve comment. The isospin mixing observed in ^{40}Ti decay will, in general, differ from that in ^{40}Ar(ν,e). However, because the total Fermi strength is conserved, any difference in the mixing will merely redistribute slightly the Fermi strength. If 5% of the Fermi strength were displaced by 50 keV (corresponding to an isospin-mixing matrix element of 11 keV) the ^{40}Ar(ν,e) cross section integrated over the ^{8}B neutrino spectrum (see below) would change by only 0.1%.

Isospin symmetry violation also produces small differences in the excitation energies of mirror ^{40}K and ^{40}Sc states. We computed the ^{40}Ar(ν,e) cross section using the

TABLE VIII. Neutrino capture cross sections for ICARUS as a function of the total energy threshold on the outgoing electron.

Threshold (MeV)	$\sigma_B(10^{-43}\,\mathrm{cm}^2)$	$\sigma_{hep}(10^{-43}\,\mathrm{cm}^2)$	$\sigma_{SN}(10^{-43}\,\mathrm{cm}^2)$
4.0	18.34	80.82	323.71
4.2	17.54	79.50	323.54
4.4	16.70	78.96	322.81
4.6	15.83	77.83	322.66
4.8	14.92	76.88	321.67
5.0	14.02	75.08	320.77
5.2	13.06	74.78	320.57
5.4	12.11	72.96	319.15
5.6	11.16	72.17	318.86
5.8	10.22	71.04	317.79
6.0	9.30	68.55	316.24

isobaric correspondences suggested in Table VII; when such correspondences could not be made we used the excitation energies of the mirror ^{40}Sc state instead. We established an upper limit on the potential errors in this process by recalculating the cross section using ^{40}Sc energies for all levels except for the two lowest daughter states and the Fermi transition. The total cross section changed by only 0.4%.

Finally, we considered the error arising from $^{40}\mathrm{Ar}(\nu,e)$ transitions to high-lying daughter levels whose analogs were not seen in our study of ^{40}Ti decay. Because ^{40}K becomes unbound to $^{39}\mathrm{K}+n$ at $E_x=7.80$ MeV, levels up to this energy could contribute to the ICARUS neutrino absorption counting rate. One can correct the neutrino absorption efficiency for these events by performing detailed Monte-Carlo calculations. But it should be mentioned that this effect is small, from the shell-model [4] cross section for capture of ^{8}B ν's to ^{40}K states with E_x between 6.4 and 7.8 MeV is only 0.13×10^{-43} cm^2, or only 0.9% of our total cross section.

None of the systematic errors considered here was large enough to warrant a correction.

IV. CONCLUSIONS

We measured the half-life and absolute transition strengths of ^{40}Ti β decay by studying β-delayed protons and γ's. We observed 21 β transitions that accounted for a summed branching ratio of $99.00\pm1.59\%$. The integrated Gamow-Teller strength of $\Sigma B(\mathrm{GT})=5.52\pm0.20$ is 28.9% of the two-particle–two-hole ''sum rule'' of $3g_A^2|N-Z|=19.1$. Our results differ significantly from those obtained in recent experiment at GSI [11]; we observed 21 β branches, they saw only 11 branches of which only 7 can be associated with our transitions. For a number of these 7 transitions, neither the energies nor the strengths agree particularly well with our values.

We used our β-decay results to compute the efficiency of the proposed ICARUS II liquid ^{40}Ar neutrino detector, and found that GT transitions, which were neglected in the original discussion of the detector efficiency, are responsible for about 73% of the neutrino-absorption cross section for ^{8}B neutrinos. A recent shell-model prediction [4] of the $^{40}\mathrm{Ar}(\nu,e)$ cross section for ^{8}B neutrinos is about 22% lower than our empirical value. The disagreement mainly arises because the shell model predictions for the daughter state excitation energies are too high. We find that the cross sections averaged over astrophysically important spectra are quite sensitive to the exact value of the energy threshold on the outgoing electrons.

Our ^{40}Ti β-decay data, when compared to $^{40}\mathrm{Ar}(p,n)$ measurements, will test the accuracy of (p,n) probes of Gamow-Teller strength in a way that complements the related test in $A=37$ [6]. The $A=37$ system has a large number of weak $[B(\mathrm{GT})<0.1]$ transitions; the $A=40$ system has two transitions with $B(\mathrm{GT})\gtrsim1$ which will permit a test for strong transitions as well. An $^{40}\mathrm{Ar}(p,n)$ experiment was recently performed at IUCF [30] but the data are not yet analyzed.

ACKNOWLEDGMENTS

This work was supported by Training and Mobility of Researchers Program of the Commission of the European Communities under Contract No. ERBFMBICT950394. The Notre Dame researchers were supported by the NSF and the Warren Foundation. The University of Washington workers were supported by the U.S. DOE. We thank the staff at GANIL for providing a high-quality beam and Hans Bichsel for electron energy-loss calculations.

[1] ICARUS Collaboration, Proposal, ICARUS II, A second-generation proton decay experiment and neutrino observatory at Gran Sasso (unpublished); see also URC http://www.aquila.infn. it:80/icarus/main.html
[2] J. N. Bahcall and H. A. Bethe, Phys. Rev. D **47**, 1298 (1993).
[3] V. Berezinsky, Comments Nucl. Part. Phys. **21**, 249 (1995).
[4] W. E. Ormand, P. M. Pizzochero, P. F. Bortignon, and R. A. Broglia, Phys. Lett. B **345**, 343 (1995).
[5] W. Trinder *et al.*, Phys. Lett. B **415**, 211 (1997).
[6] E. G. Adelberger, A. García, P. V. Magnus, and D. P. Wells, Phys. Rev. Lett. **67**, 3658 (1991).
[7] A. García, E. G. Adelberger, P. V. Magnus, H. E. Swanson, O. Tengblad, the ISOLDE Collaboration, and D. M. Moltz, Phys. Rev. Lett. **67**, 3654 (1991).
[8] W. Trinder, E. G. Adelberger, Z. Janas, H. Keller, K. Krumbholz, V. Kunze, P. Magnus, F. Meissner, A. Piechaczek, M. Pfützner, E. Roeckl, K. Rykazewski, W.-D. Schmidt-Ott, and M. Weber, Phys. Lett. B **349**, 267 (1995).
[9] A. García, E. G. Adelberger, P. V. Magnus, H. E. Swanson, D. P. Wells, F. E. Wietfeldt, O. Tengblad, and the ISOLDE Collaboration, Phys. Rev. C **51**, 439 (1995).
[10] C. Détraz *et al.*, Nucl. Phys. **A519**, 529 (1990).
[11] W. Liu *et al.*, Z. Phys. A **359**, 1 (1997).
[12] R. Anne and A. C. Mueller, Nucl. Instrum. Methods Phys. Res. B **70**, 276 (1992), and references therein.
[13] D. Bazin and O. Sorlin, LISE computer code (private communication).
[14] W. Shen, B. Wang, J. Feng, W. Zhan, Y. Zhu, and E. Feng, Nucl. Phys. **A491**, 130 (1989).
[15] P. M. Endt, Nucl. Phys. **A521**, 1 (1990).
[16] H. Bichsel (private communication).
[17] D. W. Marquardt, J. Soc. Ind. Appl. Math. **11**, 431 (1963).
[18] W. H. Press, S. A. Teukolsky, W. T. Vetterling, and B. P. Flannery, *Numerical Recipes* (Cambridge University Press, Cambridge, 1992).
[19] A. Honkanen *et al.*, Nucl. Phys. **A621**, 689 (1997).
[20] R. G. Sextro, R. A. Gough, and J. Cerny, Nucl. Phys. **A234**, 130 (1974).
[21] W. A. Sterrenburg, G. Van Middlekoop, and A. G. Ge Raedt, Nucl. Phys. **A290**, 220 (1977).
[22] G. Audi and A. H. Wapstra, Nucl. Phys. **A595**, 409 (1995).
[23] M. S. Antony, J. Britz, J. B. Bueb, and A. Pape, At. Data Nucl. Data Tables **33**, 447 (1985).
[24] D. H. Wilkinson, Nucl. Instrum. Methods Phys. Res. A **335**, 172 (1993); **335**, 201 (1993).
[25] D. H. Wilkinson and B. E. F. Macefield, Nucl. Phys. **A232**, 58 (1974).

[26] G. Savard, A. Galindo-Uribarri, E. Hagberg, J. C. Hardy, V. T. Koslowsky, D. C. Radford, and I. S. Towner, Phys. Rev. Lett. **74**, 1521 (1995).

[27] H. Behrens and J. Jänecke, *Numerical Tables for Beta-Decay and Electron Capture*, edited by H. Schopper, Landolt-Börnstein, New Series, Group 1, Vol. 4 (Springer-Verlag, Berlin, 1969).

[28] J. N. Bahcall and B. R. Holstein, Phys. Rev. C **33**, 2121 (1986).

[29] J. N. Bahcall and R. K. Ulrich, Rev. Mod. Phys. **60**, 297 (1988).

[30] C. D. Goodman *et al.*, IUCF experiment E390/406 (unpublished).